# Solid MRI contrast agents for long-term, quantitative in vivo oxygen sensing

Vincent H. Liu[a], Christophoros C. Vassiliou[a], Syed M. Imaad[a], and Michael J. Cima[b,c,1]

Departments of [a]Electrical Engineering and Computer Science and [c]Materials Science and Engineering and [b]The David H. Koch Institute for Integrative Cancer Research, Massachusetts Institute of Technology, Cambridge, MA 02139

Edited by Scott E. Fraser, California Institute of Technology, Pasadena, CA, and accepted by the Editorial Board March 25, 2014 (received for review January 2, 2014)

**Targeted MRI contrast agents have proven useful in research and clinical studies for highlighting specific metabolites and biomarkers [Davies GL, et al. (2013) *Chem Commun (Camb)* 49(84):9704–9721] but their applicability in serial imaging is limited owing to a changing concentration postinjection. Solid enclosures have previously been used to keep the local concentration of contrast agent constant, but the need to surgically implant these devices limits their use [Daniel K, et al. (2009) *Biosens Bioelectron* 24(11):3252–3257]. This paper describes a novel class of contrast agent that comprises a responsive material for contrast generation and an injectable polymeric matrix for structural support. Using this principle, we have designed a contrast agent sensitive to oxygen, which is composed of dodecamethylpentasiloxane as the responsive material and polydimethylsiloxane as the matrix material. A rodent inspired-gas model demonstrated that these materials are functionally stable in vivo for at least 1 mo, which represents an order of magnitude improvement over an injection of liquid siloxane [Kodibagkar VD, et al. (2006) *Magn Reson Med* 55(4):743–748]. We also observed minimal adverse tissue reactions or migration of contrast agents from the initial injection site. This class of contrast agents, thus, represented a new and complementary method to monitor chronic diseases by MRI.**

implantable sensors | molecular imaging

MRI is one of the most important clinical technologies for monitoring disease progression and is unique among imaging modalities in its ability to gather both high-resolution anatomical images and physiological information in the same study (1). Targeted contrast agents are useful for highlighting specific molecules in the body (2), whereas responsive contrast agents enable quantitative diagnostics using MRI. The concentration of contrast agents decreases over time owing to systemic clearance (3); some magnetic resonance (MR) methods, such as dynamic contrast-enhanced imaging, exploit this clearance of contrast agent to make inferences about the underlying physiology. Some applications, however, require a consistent concentration of contrast agent for repeatable, accurate, and quantitative measurements (4), and an internal control must be added to account for the time-changing concentration. Repeat measurements to track the progression of disease or the response to treatment also require a new bolus injection of contrast agent. These additional injections introduce uncertainty in the measurements, and the safety of long-term exposure to the contrast agent must be investigated. We describe a novel solid contrast agent that eliminates these issues to enable longitudinal imaging sensitive to oxygen. It consists of a contrast agent embedded in an injectable polymeric matrix where the matrix ensures the retention of sensitive agents in the target tissue for extended periods of time. We believe that these agents will find use in clinical medicine by enabling quantitative measurements of specific local metabolites in chronic conditions.

One area where longitudinal imaging can affect clinical decision making is sensing of local oxygen tension. Oxygen plays an important role in many pathological processes, such as cancer (5), peripheral vascular disease (6), and wound healing (7). Oxygen delivery in cancer can be limited transiently by perfusion interruption or chronically by increases in diffusion distance (8); both of these mechanisms result in hypoxia. Hypoxia in cancer confers resistance to radiotherapy (9, 10), impedes the action of chemotherapeutic agents (11), and promotes metastasis (12). Recent studies have attributed the low efficacy of drugs designed to target hypoxia to the lack of a suitable companion diagnostic assay (13–15). A diagnostic assay for selecting appropriate patients for hypoxia-targeted treatment or doses for radiotherapy would need to report oxygen status in the tumor at multiple time points during the course of treatment, because the tumor oxygen tension is dynamic and changes in response to treatment (16). There is a need for an oxygen assay that can provide oxygen information in the same location so that follow-up data can be used to evaluate treatment efficacy. Earlier attempts to measure oxygen with polarographic needle oxygen electrodes provided important evidence of hypoxia in human tumors, but oxygen electrodes have limited clinical applications owing to the invasiveness of the measurement procedure (17). Technologies currently used in the clinic for monitoring oxygen are only useful in areas with sufficient blood flow [pulse oximetry (18)], that are close to the surface [transcutaneous oximetry (19)], or that have limited changes in oxygen tension [fiber optic probes (15)]. Magnetic resonance methods, such as electron paramagnetic resonance (20) and $^{19}$F oximetry (21), provide direct measurement of local oxygen tension but require specialized equipment not currently present in most medical centers. Other MR technologies, such as blood-oxygen-level-dependent and tissue-oxygen-level-dependent

## Significance

**Information on tissue oxygen tension is critical to the successful treatment of many human diseases. Clinical decisions for diseases such as cancer benefit from knowing how oxygen tension changes in response to treatment. Acquiring this knowledge obviously requires a series of measurements and is limited currently by the use of invasive oxygen electrodes. We have developed an oxygen-sensitive MRI contrast agent for chronic oxygen tension measurements. This contrast agent can be delivered with a small-gauge needle that is minimally invasive, and subsequent measurements are entirely noninvasive. The material is stable in the body for at least 1 mo, and we envision that other types of responsive contrast agents can be used with this technology to detect different metabolites.**

Author contributions: V.H.L., C.C.V., S.M.I., and M.J.C. designed research; V.H.L. and S.M.I. performed research; V.H.L. and C.C.V. analyzed data; V.H.L. and C.C.V. wrote the paper; and M.J.C. initiated the project.

The authors declare no conflict of interest.

This article is a PNAS Direct Submission. S.E.F. is a guest editor invited by the Editorial Board.

[1]To whom correspondence should be addressed. E-mail: mjcima@mit.edu.

This article contains supporting information online at www.pnas.org/lookup/suppl/doi:10.1073/pnas.1400015111/-/DCSupplemental.



www.pnas.org/cgi/doi/10.1073/pnas.1400015111

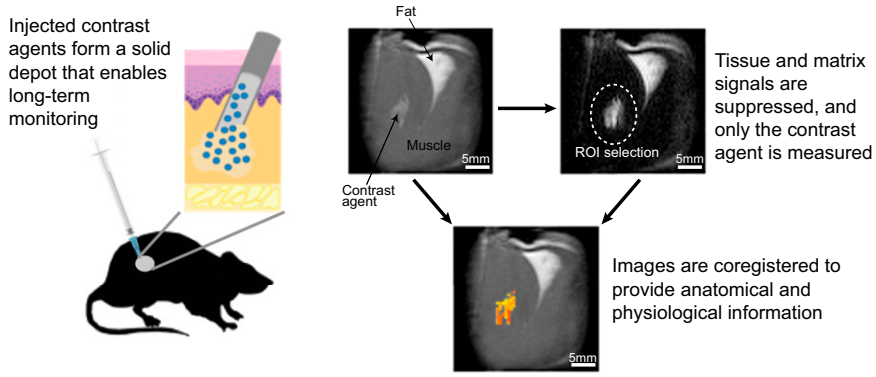


**Fig. 1.** The concept presented in this paper. The solid MRI contrast agents enable signal retention by enclosing the responsive material in a polymeric matrix. Signal from the matrix material and muscle tissue background can be suppressed with appropriately chosen pulse sequence parameters, and unwanted signal is excluded with proper region of interest (ROI) selection. An automated script then calculates the relaxation times and extracts the metabolite concentrations. This metabolic information can be overlaid on anatomical features as shown in the figure.

contrast imaging, are qualitative in nature and do not report absolute tissue oxygen tension (15, 22).

MRI contrast agents are compatible with existing equipment in the clinic, but the clearance of the contrast agent prohibits long-term monitoring. Several technologies have previously been developed to compensate for variations in contrast agent concentration (23). These methods typically require measurement of multiple parameters or established perfusion models to compensate for the concentration changes (24). Our matrix-embedded contrast agent performs measurements independently of perfusion, is not cleared, and shows no loss in performance after 1 mo in vivo.

## Results and Discussion

The contrast material is composed of two components: The first is a polymeric matrix that serves as structural support, and the second is a contrast material that generates the response to the target analyte (Fig. 1). The polymeric matrix forms a depot once injected that retains the responsive material for long durations (1 mo or more). The depot can then be interrogated using clinical MR imagers with standard clinical pulse sequences. Signal from the responsive material is isolated from the signal from the matrix material and surrounding tissue using fat or water suppression sequences. The contrast agent concentration remains constant, so the variation of contrast agents is eliminated; no additional controls are needed.

A contrast material for oxygen must not cause any adverse reaction to the surrounding tissue, nor should it be affected by tissue motion or physical stress. Additionally, it needs to respond quickly and reversibly to changes in oxygen tension. Molecular oxygen is paramagnetic and reduces the longitudinal relaxation time of the hydrogen nuclei on neighboring molecules (*Supporting Information*, section S1). The longitudinal relaxation time of linear siloxanes has previously been reported to vary with oxygen partial pressure (25), and we exploit this property and use the materials to measure oxygen tension. The MR signals obtained from siloxanes are dependent on oxygen partial pressure and are used directly for the measurements, unlike metal-ion based contrast agents that modulate the relaxivity of surrounding water protons. A panel of four linear siloxane molecules with two to five silicon atoms was screened for oxygen sensitivity over the physiologically relevant range of 0–760 mmHg. The siloxanes respond to changes in oxygen partial pressure quickly and reversibly. The longitudinal relaxation rates, $T_1^{-1}$, of these materials are proportional to the concentration of dissolved oxygen and are linear in their response to oxygen partial pressure as shown in Fig. 2.

The matrix for supporting the contrast agent must also not cause an adverse tissue response. Polydimethylsiloxane (PDMS) was chosen as a suitable polymeric matrix for the siloxanes. It is biocompatible, inert, and tolerant to a variety of fabrication methods. PDMS is also highly permeable to oxygen and is miscible with the linear siloxanes. Thus, it is not expected to inhibit oxygen diffusion into the siloxane.

Although the rf pulse used in these studies excites the protons in both PDMS and low-molecular-weight siloxanes (Fig. S1), the PDMS signal is eliminated using a spin-echo sequence with long echo time. PDMS, similar to many polymer materials, has a low transverse relaxation time, $T_2$. The signal from PDMS decays rapidly owing to its low $T_2$ and only comprises a minimal portion of the overall acquired signal under this long-echo condition; PDMS is thus rendered "transparent" (Fig. 3*A*). The long relaxation time of the embedded siloxane is preserved, and there is minimal contribution from the PDMS to the overall relaxation time. This property was verified by comparing the $T_1$ of neat siloxanes to that of 70% siloxanes incorporated in PDMS (Fig. 3*B*). Both formulations have similar relaxation times that are

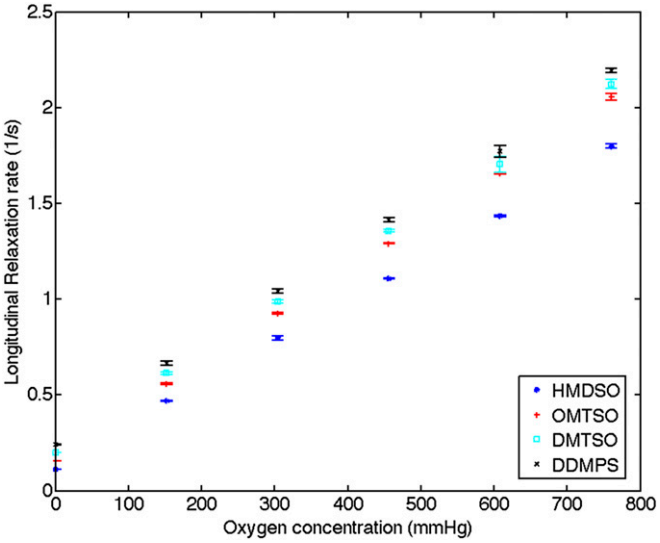


**Fig. 2.** The longitudinal relaxation rates of the four linear siloxanes change linearly with oxygen partial pressure ($n$ = 3). Error bars denote SDs. Relaxation rates were measured on Bruker Minispec at 20 MHz and 40 °C. DDMPS, dodecamethylpentasiloxane; DMTSO, decamethyltetrasiloxane; HMDSO, hexamethyldisiloxane; OMTSO, octamethyltrisiloxane.

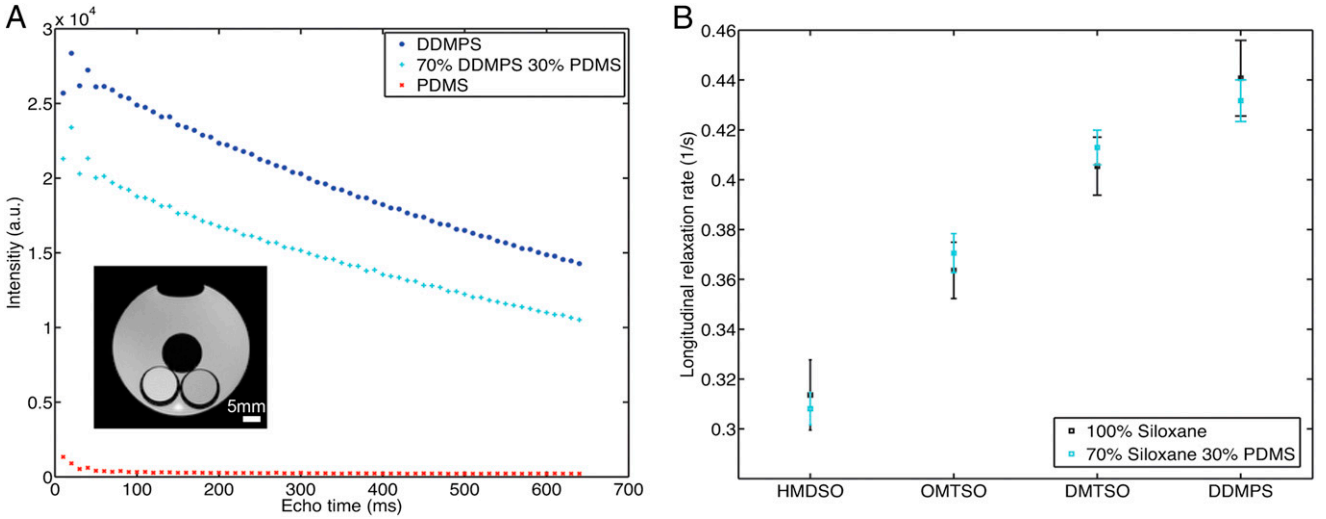


**Fig. 3.** The signal from PDMS can be suppressed by choosing an appropriately long echo time. (*A*) MRI scans of phantoms containing different siloxanes. The phantoms were in glass tubes and were immersed in a container filled with DI water to minimize magnetic susceptibility differences. PDMS has a $T_2$ of 20 ms at 7 T, and the average Intensity of PDMS phantom drops to less than 20% of its initial value at an echo time of 100 ms. Coupled with a lower initial intensity value, signal from PDMS would constitute less than 1% of acquired signal at 100 ms; 70% DDMPS 30% PDMS phantoms have lower intensity values throughout the measurement period owing to an effectively smaller amount of sample but the extracted $T_2$ value is not significantly different from pure DDMPS. (*Inset*) Representative image of phantoms acquired using an echo time of 100 ms. The image was obtained from an axial slice and shows a cross-sectional view of the phantoms. Top, PDMS; bottom left, DDMPS; bottom right, 70% DDMPS 30% PDMS. (*B*) Comparison between neat siloxane and siloxane incorporated into PDMS at 70 wt/wt percent in air ($n = 3$). The relaxation rates of neat siloxane material are not significantly different from material incorporated into PDMS, indicating that signal from the PDMS matrix can be effectively suppressed. The data points are based on six measurements in the MRI at 37 °C and error bars represent SDs of measurements.

much longer than the $T_1$ of PDMS. The two materials can, therefore, be optimized independently: The matrix can be selected for its physical properties and its ability to retain the sensing agent, and the linear siloxane can be chosen to optimize the oxygen measurement.

We selected dodecamethylpentasiloxane (DDMPS) as the contrast material for in vivo experiments because its shorter relaxation time reduces the scan time and the overall study duration. The oxygen response of DDMPS embedded in PDMS was characterized using MRI, and its calibration curve from 0–760 mmHg oxygen partial pressure was acquired at three different temperatures. The measured longitudinal relaxation rate of the embedded DDMPS is linear with oxygen partial pressure (Fig. S2), which is similar to liquid DDMPS. Our results show that a change of less than 15 mmHg oxygen partial pressure near the hypoxic levels can be reliably detected (*Supporting Information*, section S2). The sensitivity is limited by the accuracy with which the relaxation time can be measured, which can be improved by increasing the acquisition time or increasing the voxel size. The response kinetics of embedded DDMPS is comparable to the liquid siloxanes and steady state is reached in less than 10 min (Fig. 4). The response kinetics were captured by recording the image intensity every 2 min; the intensities were normalized relative to the first image in the series.

We also tested DDMPS retention in the PDMS matrix by examining the weight change of embedded DDMPS over time (Fig. S3). Whereas DDMPS gradually escapes from the devices exposed to air, devices immersed in deionized water and FBS at 37 °C for over a month showed less than 1% weight change. The lack of weight loss for sensors placed in an aqueous environment can be attributed to the low solubility of siloxanes in those solutions. Thus, the aqueous solution creates a barrier for transport of low-molecular-weight siloxanes into the headspace of the container. Although it is not possible to quantify the amount of siloxane retained in vivo, this result suggests that the siloxane will be retained long-term in the body. We tested device stability for a month in vivo by monitoring its performance as a sensor, as described below.

An inspired-gas model in rats was used to compare the stability of our sensors to results published in the literature on conventional liquid contrast agents. Inspired-gas change is a reliable method for establishing different oxygen tensions in vivo and provides a reference point for different studies (26). Fig. 5*A* shows the data acquired in an experiment performed 30 min after sensor injection. It can be seen that the particles formed a depot after injection. Depot formation was achieved via a filtration mechanism and no specific interaction with PDMS was required. The particles coalesce into a single sensor once the saline has filtered into the surrounding tissue. Most tissue has sufficient connective matrix to act as an appropriate filter, but these sensors are not suitable for injection into arterial, venous, or cerebrospinal fluid. The measurement results correlate well

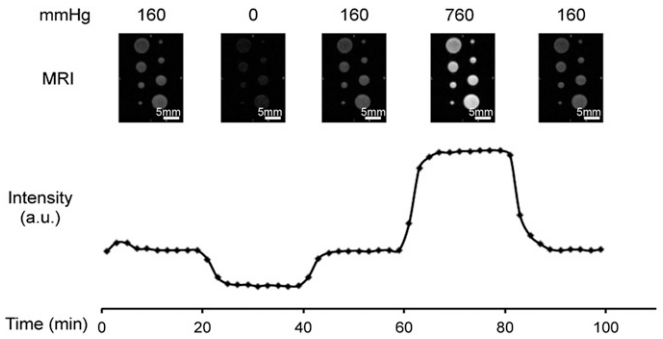


**Fig. 4.** Kinetics of response of 70% DDMPS 30%PDMS phantoms are similar to liquid DDMPS. These phantoms were exposed to changing oxygen partial pressure in the MRI, and image intensity was used as a surrogate indicator of $T_1$. Images were taken every 2 min with a coronal orientation and the intensity in the phantoms was averaged to estimate time to steady state. We found that steady state was achieved in less than 10 min for phantoms of all sizes.

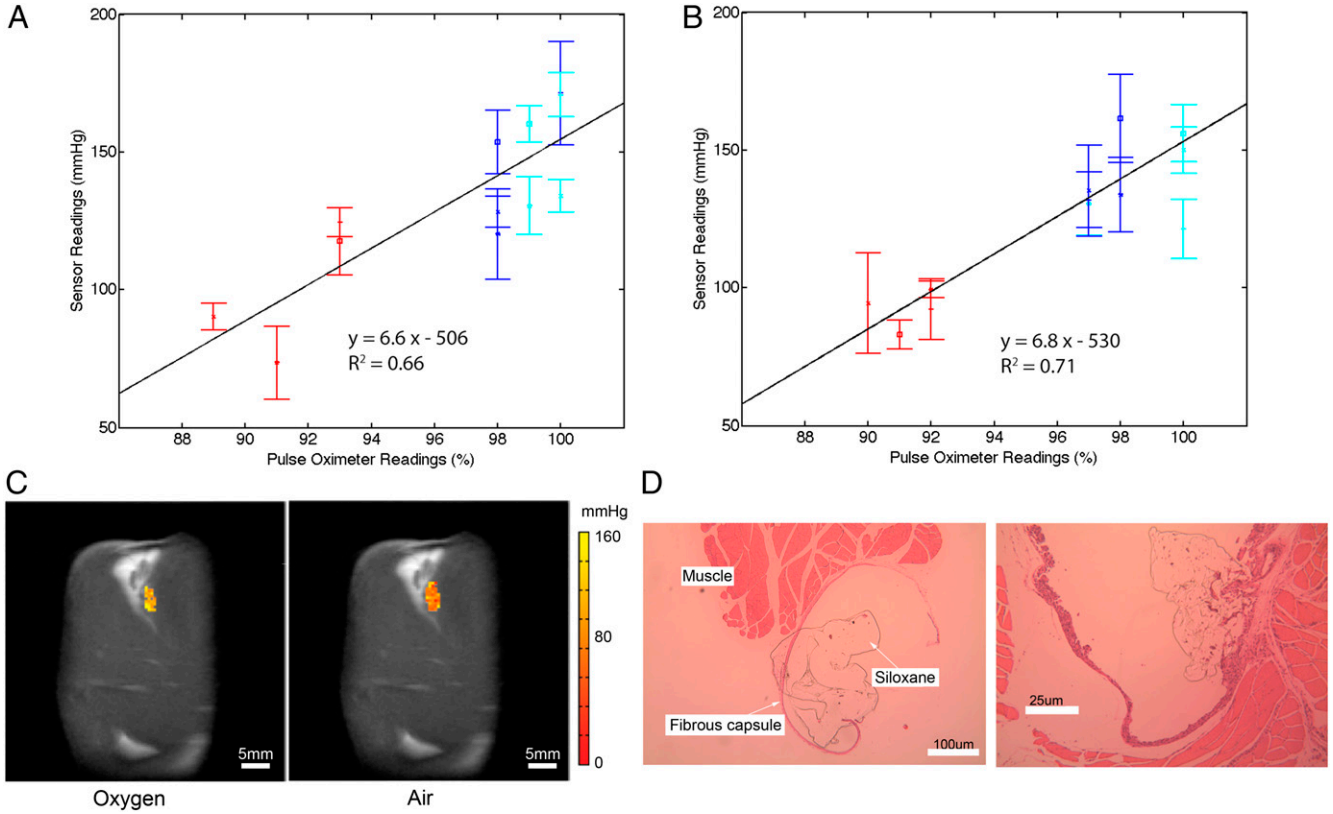


**Fig. 5.** The contrast agents are stable and biocompatible for at least 1 mo. The depots of contrast agent formed reliably in different animals, but the exact shape or size of the depots differed between animals because these physical parameters were altered by the specific tissue structures and how quickly the saline was cleared. (*A* and *B*) Oxygen measurements extracted from sensors immediately after injection (*A*) and 4 wk after injection (*B*) are plotted against pulse oximeter measurements ($n = 4$). Each data point represents an average of six measurements in each animal and error bars denote SDs of measurements. A linear regression line is used to find the correlation between sensor measurements and pulse oximeter readings. The values of the regression slopes are similar in both measurements, indicating similar correlation between pulse oximeter readings and sensor measurements over the 4-wk period. Deviations from the line are likely due to variations in local tissue oxygen level and differences in injection location. Blue, oxygen (initial); red, air; cyan, oxygen (reverse). (*C*) Maps of extracted oxygen tension can be overlaid on anatomical images to provide both physical and biochemical information. These two representative MRI images are coronal slices of the leg and are taken from animals breathing oxygen (*Left*) and air (*Right*). (*D*) H&E-stained micrographs showed that the 70% DDMPS/PDMS microparticles fused into a depot that resisted migration after injection. There is minimal foreign body reaction to the injected microparticles as evidenced by the thin fibrous capsule surrounding the injection site.

with the expected changes in tissue oxygen level in each animal, and sensor $T_1$ started changing within 5 min of inspired-gas switch and reached steady state within 10 min.

We examined the functional stability of the injected sensors by repeating the inspired-gas experiment with the same animals 4 wk postinjection. The kinetics of response of the injected sensors was the same as and correlation with pulse oximetry readings was similar to (Fig. 5*B*) the previous set of experiments. Liquid siloxanes directly injected into a tissue site have a half-life of 35 h as reported in a recent paper by Kodibagkar et al. (25). Neither the kinetics nor dynamic range of the sensors was reduced over the 4-wk period, suggesting at least one order of magnitude improvement over a simple liquid contrast agent injection. The MRI slice orientation may vary slightly between studies, but we do not expect the overall shape of the sensor to have changed over the implantation period. The measurement is also not dependent on the shape of the depot because we only need sufficient volume to measure the $T_1$ of the material. The rat muscle was excised 4 wk after injection for histological examination. The solid depot of injected sensors can be seen wedged in between muscle fibers, and there was minimal evidence of inflammatory reaction or fibrous capsule formation after the particles were implanted for 4 wk (Fig. 5*C*). The lack of sensor migration or performance degradation is essential for long-term monitoring because it ensures that the same region is measured in subsequent imaging sessions.

We simulated the effects of compressive injury with a hindlimb ischemia model. An inflatable pressure cuff restricted blood flow to the limb and increased the local compartment pressure. This model tested the variability of the injected sensors with changes in blood flow and when subjected to movement and physical stress. Previous studies have shown transcutaneous oxygen tension measurements to be susceptible to factors such as local blood flow and arterial oxygen content (19, 27), and we found that the pulse oximeter readings became unstable when circulation was restricted. The contrast agents described in this paper directly detect decreased oxygen levels caused by the increased compartment pressure (Fig. 6) and are unaffected by changes in blood flow. The depot of contrast agents was not damaged or displaced when the compartmental pressure was elevated, making the sensor suitable for use in locations where movement or physical stress is expected.

We have shown that these materials provided a way to accomplish long-term monitoring of oxygen tension in vivo. These injectable solid contrast agents allow for monitoring of specific tissue sites independently of blood flow compared with other MR-based approaches. This should allow clinicians to monitor regions with poor perfusion or conditions involving compromised

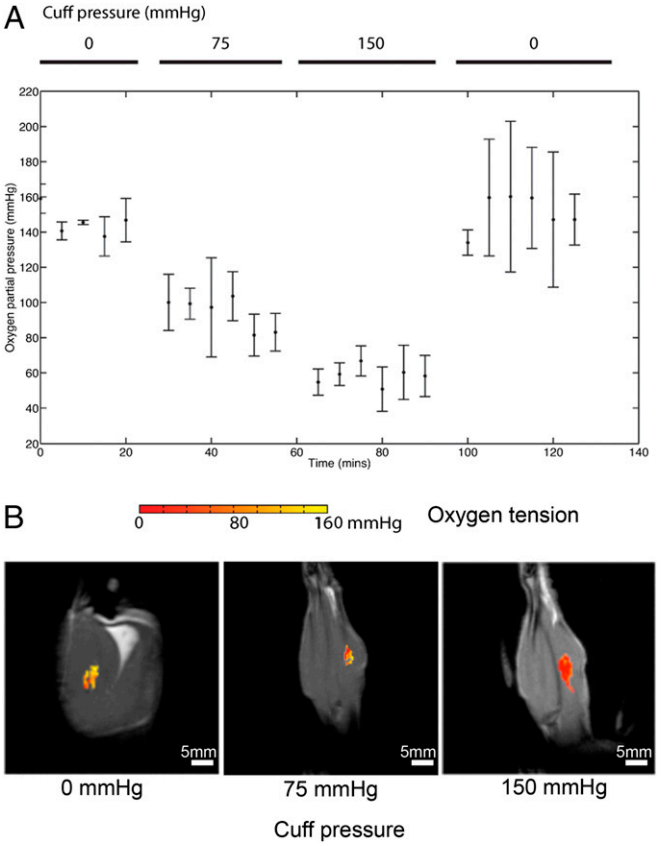


**Fig. 6.** The injected contrast agents resisted physical stress and continued functioning irrespective of blood flow. (*A*) Oxygen tension extracted during circulation restriction experiment ($n$ = 3). Error bars denote SDs across different animals. Pulse oximeter readings become unavailable when the pressured was raised to 75 mmHg and 150 mmHg pressure levels and are not presented here. The oxygen level was observed to return to the initial level after the pressure cuff was released. (*B*) Representative pixel maps of extracted oxygen tension are overlaid with MRI scans of the animal at different cuff pressure levels. The pictures are coronal slices of the animal's leg. Sensor migration, even at the highest pressure level applied, was not observed.

blood flow. We have additionally demonstrated that these sensors would stay functional in the same tissue site for at least 4 wk; this allows for longitudinal imaging to monitor the same tissue site and eliminate possible spatial or temporal variations of contrast agent concentration.

The polymeric matrix retains the contrast agent in the local tissue site and lends biocompatibility to the sensor. Silicones are among the most widely used biomaterials and have demonstrated excellent safety profile in vivo (28). It is the matrix that determines the physical properties of the sensors, and it should be selected based on its physical properties and compatibility with the responsive contrast material. The signal from the material can be eliminated with appropriate pulse sequence parameters to ensure maximum contrast from the sensitive agent.

Whereas this paper demonstrated a solid contrast agent for measuring oxygen tension, the same concept can be extended for use with other responsive contrast agents. A variety of contrast agents have been used in MRI studies to highlight tissue structures; "smart" contrast agents, designed to respond to changing environmental conditions, are gaining importance in both the research and clinical community (29). Targets of these contrast agents include specific metabolites such as oxygen (25) and pH (30) and proteins involved in enzymatic reactions (31). Similarly, a number of biocompatible polymers, in addition to the silicones used in this study, could be used to hold these contrast agents in place.

Some of the potential applications listed require different sets of contrast agents or polymeric matrices to be implemented. Two design criteria need to be satisfied for successful implementation of this concept. The first criterion is a matrix that retains the contrast agents (i.e., with favorable partition coefficient) and is permeable to the analyte of interest. The second criterion involves a mechanism for contrast generation. Oxygen molecules are inherently paramagnetic and increase relaxation rate of surrounding molecules, but other responsive contrast agents can be used with analytes that are nonmagnetic to enable their detection. An important point of consideration in designing these contrast agents is that they should be compatible with existing medical practices and equipment. Importantly, proton MRI scanners are readily available in most medical centers. The long-term retention of the sensor can also be used to mark a specific location within the body. Fiducial markers, commonly used to mark a location for serial imaging or treatment sessions (32), can potentially be used to provide chemical information in addition to a spatial reference point with the concept described in this paper.

## Materials and Methods

**Contrast Agent Synthesis.** Sylgard 184 from Dow Corning was used to form the support matrix for the siloxanes. After a 10:1 mixture of vinyl-terminated PDMS base/curing agent was prepared, liquid siloxane (Sigma–Aldrich) was added to the mixture to form a solution of PDMS/siloxane. This solution was then heat-cured at 80 °C for 90 min to form fully cross-linked PDMS devices with liquid siloxanes contained within.

Microparticles were created as an oil-in-water emulsion. The PDMS/siloxane base solution was first added to a deionized (DI) water solution of 5 wt/wt percent Vitamin E-TPGS (Sigma–Aldrich). The final mixture consisted of 30% (vol/vol) of siloxanes in water with a total volume of 10 mL. This mixture was then subjected to high shear forces with a tissue homogenizer (Silverson Machines) to form a suspension of PDMS/siloxane microparticles. The homogenizer was run at 5,000 rpm for 4 min with a high shear screen and a square-hole work head. The resulting emulsion was then heat-cured under stirring in a water bath at 65 °C overnight to form solid microparticles (Fig. S4).

The particles were washed three times with DI water to remove the excess surfactants. The particles were first centrifuged at 600 × $g$ for 5 min. The supernatant was then removed with a Pasteur pipette. DI water was then added back to the container at a 10:1 volume ratio of DI water: particles and then vigorously mixed with the particles. The particles were resuspended in sterile saline before injection.

**Relaxation Time Measurement.** Proton relaxation times were measured using a benchtop NMR relaxometer (Minispec mq20; Bruker) with a 0.47-T static field. Relaxation rates were measured using an inversion recovery pulse sequence with the signal intensity measured at 13 recovery times. Intensity data averaged over four scans were fitted to the equation $I = I_0\left(1 - 2e^{-\frac{t}{T_1}}\right)$ to extract the relaxation time.

**MRI.** MRI was performed using a 7-T small animal imager (Agilent). The imaging protocol included a scout pulse sequence for locating devices and a fast spin-echo sequence with inversion recovery for performing $T_1$ measurements with the following parameters: matrix size = 64 × 64, field of view = 32 mm × 32 mm, slice thickness = 2 mm, echo time (TE) = 12.5 ms, echo train length = 16, and kzero = 8. The effective TE of sequence used was 100 ms. Repetition time was adjusted depending on the $T_1$ of particular samples and was set to at least 3× measured $T_1$. Eight inversion times, separated exponentially, were used to generate data for $T_1$ mapping. The measurements were performed in a quadrature volume coil that measures 63 mm in diameter. The excitation pulse and refocusing pulses had a 3-kHz bandwidth, and the receiver bandwidth was 100 kHz. No presaturation pulses were applied for these studies.

**Gas Composition Modulation.** A gas mixer was used to produce a gas stream with different oxygen concentrations for these experiments. Nitrogen was used as a balance gas for a preset amount of oxygen in the gas stream (i.e., a 21% oxygen gas stream would be balanced with a 79% of nitrogen). The

gas mixer contains a flow meter and feedback system to ensure that the composition of the gas stream stays constant.

**Sensor Injection.** The sensor in these experiments was formed by injecting a 30-μL bolus of 70% DDMPS 30% PDMS microparticles into the calf muscle of Sprague–Dawley rats. This particles suspension had a solid fraction of roughly 66% vol/vol. The microparticles aggregated into a depot that became a single sensor once injected. Because ∼20 μL of solid material was present in the depot, the equivalent spherical diameter is 1.68 mm. A pulse oximeter clipped to the rat toe provided a secondary indicator of oxygen level in the rats.

**Inspired-Oxygen Experiment.** All experiments were conducted in accordance with the guidelines of the Committee on Animal Care at Massachusetts Institute of Technology. The rats were anesthetized using 2% isoflurane in oxygen. Microparticles consisting of 70% DDMPS and 30% PDMS were injected into the calf muscle of each rat. The rats were placed into the MRI under anesthesia after contrast agent injection. Each rat was imaged for 1.5 h with the experiment divided into three segments: a baseline measurement for the first 30 min with the rat breathing oxygen, then an experimental measurement for 30 min with the rats breathing medical air, and finally recovery measurement for 30 min with the rats breathing oxygen. The rats were scanned every 5 min and monitored to ensure proper respiration and heart rate throughout the experiment. An MR-compatible forced warm air circulator maintained the animals' body temperature throughout the imaging study.

**Hind-Leg Compression Study.** An inflatable pressure cuff was placed proximal to the injection site on the rat's leg and was inflated after a baseline measurement was taken. The pressure was applied in a stepwise pattern, first increasing from 0 mmHg to 75 mmHg and then to 150 mmHg. A pulse oximeter on the rat's toe served as a secondary oxygen indicator similar to the inspired-gas experiments.

**MRI Data Analysis.** The voxels containing the contrast agents were isolated using specific MRI pulse sequence parameters and postprocessing with MATLAB. The tissue background was minimized with a pulse sequence with long TE; this allows a script written in MATLAB to automatically extract the intensity of pixels containing the sensor. The script identifies the pixels containing contrast agent by differentiating areas with high intensity from areas with low intensity in a selected area of interest. The area of interest selection was done by the user to approximate the location of the injected contrast agents to ensure selection of the correct pixels.

Once the voxels corresponding to the siloxane depot were identified, the data were analyzed in two different manners. The first approach treats each pixel independently as an individual sensor. The intensity of each pixel is mapped to the inversion recovery equation to $I = \left| I_0 \left( 1 - f_{inv} e^{\frac{-t}{T_1}} \right) \right|$ using MATLAB to obtain the longitudinal relaxation time. $f_{inv}$ represents the effective fraction of inverted protons and accounts for equipment or pulse sequence imperfections (33). A $T_1$ map resulting from this analysis can then be converted to give a map of oxygen partial pressure. The map can also be overlaid on anatomical features to relate oxygen partial pressure to tissue structures. The second approach treats the injected contrast agents as a single sensor. Intensity was averaged across the selected pixels and was fitted to the same equation using MATLAB. This relaxation time can then be converted to oxygen partial pressure with a calibration curve.

**ACKNOWLEDGMENTS.** This work was supported by National Cancer Institute Centers of Cancer Nanotechnology Excellence Grant 5U54CA151884-03 and United States Army Research Office Grant W911NF-13-D-0001.

1. Strijkers GJ, Mulder WJ, van Tilborg GA, Nicolay K (2007) MRI contrast agents: Current status and future perspectives. *Anticancer Agents Med Chem* 7(3):291–305.
2. Bulte JW, Kraitchman DL (2004) Iron oxide MR contrast agents for molecular and cellular imaging. *NMR Biomed* 17(7):484–499.
3. Longmire M, Choyke PL, Kobayashi H (2008) Clearance properties of nano-sized particles and molecules as imaging agents: Considerations and caveats. *Nanomedicine (Lond)* 3(5):703–717.
4. Geraldes CF, Laurent S (2009) Classification and basic properties of contrast agents for magnetic resonance imaging. *Contrast Media Mol Imaging* 4(1):1–23.
5. Höckel M, Vaupel P (2001) Tumor hypoxia: Definitions and current clinical, biologic, and molecular aspects. *J Natl Cancer Inst* 93(4):266–276.
6. Wyss CR, Matsen FA, 3rd, Simmons CW, Burgess EM (1984) Transcutaneous oxygen tension measurements on limbs of diabetic and nondiabetic patients with peripheral vascular disease. *Surgery* 95(3):339–346.
7. Gordillo GM, Sen CK (2003) Revisiting the essential role of oxygen in wound healing. *Am J Surg* 186(3):259–263.
8. Vaupel P, Dossel O, Schlegel W (2009) Causes, detection and characterization of tumor hypoxia. *World Congress on Medical Physics and Biomedical Engineering,* Vol 25, Pt 13:32–35.
9. Bertout JA, Patel SA, Simon MC (2008) The impact of O2 availability on human cancer. *Nat Rev Cancer* 8(12):967–975.
10. Melillo G, ed (2014) *Hypoxia and Cancer: Biological Implications and Therapeutic Opportunities* (Springer, New York).
11. Teicher BA, Lazo JS, Sartorelli AC (1981) Classification of antineoplastic agents by their selective toxicities toward oxygenated and hypoxic tumor cells. *Cancer Res* 41(1):73–81.
12. Hong WK, et al. (2010) *Holland-Frei Cancer Medicine* (People's Medical Publishing House, Shelton, CT), 8th Ed, p xxv.
13. Rajendran JG, Krohn KA (2005) Imaging hypoxia and angiogenesis in tumors. *Radiol Clin North Am* 43(1):169–187.
14. Rischin D, et al. (2010) Tirapazamine, cisplatin, and radiation versus cisplatin and radiation for advanced squamous cell carcinoma of the head and neck (TROG 02.02, HeadSTART): A phase III trial of the Trans-Tasman Radiation Oncology Group. *J Clin Oncol* 28(18):2989–2995.
15. Mason RP, et al. (2010) Multimodality imaging of hypoxia in preclinical settings. *Q J Nucl Med Mol Imaging* 54(3):259–280.
16. Moulder JE, Rockwell S (1987) Tumor hypoxia: Its impact on cancer therapy. *Cancer Metastasis Rev* 5(4):313–341.
17. Clark LC, Jr., Misrahy G, Fox RP (1958) Chronically implanted polarographic electrodes. *J Appl Physiol* 13(1):85–91.
18. Chan ED, Chan MM, Chan MM (2013) Pulse oximetry: Understanding its basic principles facilitates appreciation of its limitations. *Respir Med* 107(6):789–799.
19. Peabody JL, Willis MM, Gregory GA, Tooley WH, Lucey JF (1978) Clinical limitations and advantages of transcutaneous oxygen electrodes. *Acta Anaesthesiol Scand Suppl* 68:76–82.
20. Swartz HM, et al. (2004) Clinical applications of EPR: Overview and perspectives. *NMR Biomed* 17(5):335–351.
21. Hunjan S, et al. (2001) Tumor oximetry: Demonstration of an enhanced dynamic mapping procedure using fluorine-19 echo planar magnetic resonance imaging in the Dunning prostate R3327-AT1 rat tumor. *Int J Radiat Oncol Biol Phys* 49(4):1097–1108.
22. Ogawa S, Menon RS, Kim SG, Ugurbil K (1998) On the characteristics of functional magnetic resonance imaging of the brain. *Annu Rev Biophys Biomol Struct* 27:447–474.
23. Taktak S, Sosnovik D, Cima MJ, Weissleder R, Josephson L (2007) Multiparameter magnetic relaxation switch assays. *Anal Chem* 79(23):8863–8869.
24. Choyke PL, Dwyer AJ, Knopp MV (2003) Functional tumor imaging with dynamic contrast-enhanced magnetic resonance imaging. *J Magn Reson Imaging* 17(5):509–520.
25. Kodibagkar VD, Cui W, Merritt ME, Mason RP (2006) Novel 1H NMR approach to quantitative tissue oximetry using hexamethyldisiloxane. *Magn Reson Med* 55(4):743–748.
26. Gallez B, Mäder K (2000) Accurate and sensitive measurements of pO(2) in vivo using low frequency EPR spectroscopy: How to confer biocompatibility to the oxygen sensors. *Free Radic Biol Med* 29(11):1078–1084.
27. Scheffler A, Rieger H (1992) Clinical information content of transcutaneous oxymetry (tcpO2) in peripheral arterial occlusive disease (a review of the methodological and clinical literature with a special reference to critical limb ischaemia). *Vasa* 21(2):111–126.
28. Brandon HJ, Jerina KL, Wolf CJ, Young VL (2003) Biodurability of retrieved silicone gel breast implants. *Plast Reconstr Surg* 111(7):2295–2306.
29. Davies GL, Kramberger I, Davis JJ (2013) Environmentally responsive MRI contrast agents. *Chem Commun (Camb)* 49(84):9704–9721.
30. Aime S, et al. (2002) Paramagnetic lanthanide(III) complexes as pH-sensitive chemical exchange saturation transfer (CEST) contrast agents for MRI applications. *Magn Reson Med* 47(4):639–648.
31. Moats RAaFSEaMTJ (1997) A "smart" magnetic resonance imaging agent that reports on specific enzymatic activity. *Angew Chem Int Ed Engl* 36(7):726–728.
32. de Souza Lawrence L, et al. (2013) Novel applications of an injectable radiopaque hydrogel tissue marker for management of thoracic malignancies. *Chest* 143(6):1635–1641.
33. Röschmann P (1987) Radiofrequency penetration and absorption in the human body: Limitations to high-field whole-body nuclear magnetic resonance imaging. *Med Phys* 14(6):922–931.